Check for updates

Earth and Space Science

RESEARCH ARTICLE
10.1029/2024EA003971

Special Collection:
Science from the Surface Water and Ocean Topography Satellite Mission

Estimating Wind Direction and Wind Speed Over Lakes With Surface Water Ocean Topography and Sentinel-1 Satellite Observations

Katie A. McQuillan[1], George H. Allen[1], Jessica Fayne[2], Huilin Gao[3], and Jida Wang[4,5]

[1]Department of Geosciences, Virginia Polytechnic Institute and State University, Blacksburg, VA, USA, [2]Department of Earth and Environmental Sciences, University of Michigan, Ann Arbor, MI, USA, [3]Zachry Department of Civil and Environmental Engineering, Texas A&M University, College Station, TX, USA, [4]Department of Geography and Geographic Information Science, University of Illinois Urbana-Champaign, Urbana, IL, USA, [5]Department of Geography and Geospatial Sciences, Kansas State University, Manhattan, KS, USA

Abstract Wind at the water-air interface is an important driver of hydrologic and biogeochemical processes in lakes. Satellite synthetic aperture radar (SAR) is commonly used over the ocean to retrieve wind fields using backscatter coefficients which are sensitive to wind-driven surface water roughness; however, its application to lakes has been largely unexplored. Here we assess the utility of SAR to retrieve wind fields specifically for lakes. We estimated wind direction from SAR backscatter using the Modified Local Gradient method for Surface Water Ocean Topography (SWOT) and Sentinel-1 data. The estimated wind direction was then used as an input into a C-band geophysical modeling function (GMF) to invert wind speed from Sentinel-1 data. Comparisons between SWOT backscatter and in situ wind speeds were used to provide a foundation for understanding how SWOT could be used to study wind speeds. Using buoy data for validation, we found wind direction (1 km) mean absolute error (MAE) ranged from 31° to 40° for Sentinel-1 and 28° to 38° for SWOT. Sentinel-1 wind speed (100 m) MAE ranged from 1.05 to 2.09 m/s. These retrievals were more accurate and at higher resolution compared to global reanalysis dataset ERA5 (0.25°), with wind direction MAE from 23° to 50° and wind speed MAE from 1.49 to 2.35 m/s. SWOT backscatter sensitivity to wind speed depended on incidence angle, and demonstrated utility for developing a GMF for lakes. These methods could be used to better understand wind dynamics globally, especially over small lakes and in data poor regions.

Key Points:

- Synthetic aperture radar (SAR) satellites, including Surface Water Ocean Topography (SWOT) and Sentinel-1, provide useful estimates of wind speed and direction over lakes
- SAR-derived winds are more accurate, higher resolution, and captured more in-lake variability compared to a global reanalysis dataset
- SWOT backscatter relationship with wind speed shows promise for developing a wind speed model specifically for lakes

Supporting Information:

Supporting Information may be found in the online version of this article.

Correspondence to:

K. A. McQuillan and G. H. Allen,
kmcquil@vt.edu;
geoallen@vt.edu

Citation:

McQuillan, K. A., Allen, G. H., Fayne, J., Gao, H., & Wang, J. (2025). Estimating wind direction and wind speed over lakes with SWOT and Sentinel-1 satellite observations. *Earth and Space Science*, *12*, e2024EA003971. https://doi.org/10.1029/2024EA003971

Received 13 SEP 2024
Accepted 29 DEC 2024

Author Contributions:

Conceptualization: Katie A. McQuillan, George H. Allen, Jessica Fayne
Formal analysis: Katie A. McQuillan
Funding acquisition: George H. Allen
Methodology: Katie A. McQuillan, George H. Allen, Jessica Fayne
Supervision: George H. Allen

© 2025. The Author(s).
This is an open access article under the terms of the Creative Commons Attribution-NonCommercial-NoDerivs License, which permits use and distribution in any medium, provided the original work is properly cited, the use is non-commercial and no modifications or adaptations are made.

1. Introduction

Wind at the water-air interface is a major source of energy that influences lake dynamics. It is an important driver of water, gas, and energy fluxes, including evaporation and greenhouse gas exchange (Schilder et al., 2013; Zhao et al., 2024). Wind also drives lake water circulation and influences seasonal and diel thermal structures, transport, and mixing (Desai et al., 2009; Wang et al., 2020; Woolway et al., 2019). Wind induced turbulent mixing has a large influence on water quality parameters like suspended solids, total phosphorus, and chlorophyll concentrations (Jalil et al., 2019; Tammeorg et al., 2013). Therefore, spatial and temporal variability of wind over lakes is an important parameter used to understand, monitor, and predict a wide range of processes and conditions in lakes.

Wind over lakes is often represented using gridded reanalysis datasets at regional to global scales or buoy stations at point locations (Brunet et al., 2023; Trolle et al., 2012). While reanalysis datasets are useful for large-scale analyses or models that require continuous meteorological forcings (Baracchini et al., 2020; Zhao et al., 2024), they are often too coarse to capture patterns of wind variability within lakes (Brunet et al., 2023). Furthermore, the difference of wind speed over land compared to water (e.g., usually slower wind speed over land compared to water) is difficult to resolve because most lake extents are smaller than the size of a reanalysis grid cell (Messager et al., 2016). For example, global reanalysis datasets ERA5 (0.25° resolution) and MERRA-2 (0.5° resolution) are much coarser than the average lake size, estimated to be approximately 0.15 km^2 for lakes larger than one ha (Gelaro et al., 2017; Hersbach et al., 2018; Messager et al., 2016). Consequently, wind speed over water is often underestimated in reanalysis datasets (Wang et al., 2022). On the other hand, while in-situ data collected by buoys are inherently more accurate than reanalysis datasets, they are sparsely distributed point observations and therefore similarly limited in their ability to represent spatial variability of wind within lakes (Chen et al., 2004).

23335084, 2025, 3, Downloaded from https://agupubs.onlinelibrary.wiley.com/doi/10.1029/2024EA003971, Wiley Online Library on [04/04/2025]. See the Terms and Conditions (https://onlinelibrary.wiley.com/terms-and-conditions) on Wiley Online Library for rules of use; OA articles are governed by the applicable Creative Commons License

Writing – original draft: Katie A. McQuillan
Writing – review & editing: George H. Allen, Jessica Fayne, Huilin Gao, Jida Wang

The formation of wind-driven waves on lakes is sensitive to local environmental conditions. Lakes surrounded by complex topography including mountains, valleys, and coastal regions often exhibit highly dynamic winds, generating spatially variable wind-driven waves (Brunet et al., 2023; Keen & Lyons, 1978; Lemmin & D'Adamo, 1997). Additionally, the interplay between wind speed and lake morphology (e.g., size and shape) influences wave formation, resulting in different wave characteristics across lake sizes. For example, in very large lakes, like the Great Lakes of North America, strong winds act across long fetches generating large wave heights (Jin & Wang, 1998; Mao et al., 2016). Conversely, shorter and more intermittent waves are often observed on small lakes with limited fetches (Hofmann et al., 2010). Thus, in order to extract dynamic wind patterns over both large and small lakes, high resolution satellite remote sensing of wind-driven waves could provide useful information.

High-resolution SAR has been used over the ocean to estimate wind fields by analyzing radar backscatter as a measure of wind-driven surface water roughness (see review by Asiyabi et al., 2023). The most commonly used approach, using a scatterometer, models the dependency of radar backscatter on wind speed, azimuth angle with respect to wind direction, and incidence angle using a geophysical modeling function (GMF). Scatterometers invert GMFs to solve for both wind speed and direction by leveraging multiple surface water observations of the same location at nearly the same time from different viewing geometries (Chelton & Freilich, 2005; Hersbach, 2010). In contrast, SAR returns just one observation for each location from a single viewing geometry, and, therefore, cannot be used to produce a GMF or retrieve wind speeds and directions in the same way as scatterometers. To overcome this limitation, ancillary wind direction is typically supplied to the GMF in order to solve for wind speed (Jang et al., 2019; Monaldo et al., 2004). Numerical weather prediction datasets (NWPs) are typically used for the ancillary wind direction; however, they are coarse relative to the sub-kilometer resolution of SAR, which inherently limits the gains in spatial resolution.

To address the shortcomings of NWP-based wind direction estimates, multiple wind direction retrieval algorithms based on visible wind streaks in SAR imagery have been proposed (Gerling, 1986; Koch, 2004; Zecchetto, 2018). Wind streaks appear as bright and dark linear features in SAR images that are closely aligned with the mean water surface wind direction; however, they are not present in all images (Zhao et al., 2016). The Local Gradient (LG) method, a commonly used retrieval approach, extracts the dominant direction of wind streaks by computing local gradients (Koch, 2004). Although this approach has not been tested over inland lakes, it has been used extensively in coastal regions and validated using buoy and NWP datasets with a spatial resolution up to 3 km and with accuracy from approximately 10 to 40° (Bruun Christiansen et al., 2006; Koch, 2004; Rana et al., 2019; Wang & Li, 2016; Zhou et al., 2017). For example, the LG method was used to extract wind direction in the geomorphically complex Camargue and Wadden Sea coastal areas (Rana et al., 2019), during a typhoon in the west Pacific (Wang & Li, 2016), and in the Sogne Fjord in Norway (Koch, 2004), demonstrating its promise for application to lakes.

Very few studies have utilized radar returns to investigate any part of the wind field over lakes. The application of coarse scatterometers (12.5–25 km) to lakes has been successful. For example, Nghiem et al. (2004) used SeaWinds Scatterometer to retrieve wind speed and direction with reasonable accuracy over the Great Lakes where NOAA currently provides wind on an operational basis as the Metop-C ASCAT dataset. In comparison, the application of high-resolution SAR (<100 m) has been more limited. Two studies have applied Sentinel-1 SAR images across a handful of lakes to retrieve wind speed with reasonable accuracy (Katona & Bartsch, 2018; Sergeev et al., 2023). Katona and Bartsch (2018) developed a model to predict wind speed dependent on Sentinel-1 backscatter and incidence angle using exponential functions. They opted not to include wind direction due to the coarseness of available products relative to lake size. Sergeev et al. (2023) developed a two-scale composite model for wind speed over Gorsky reservoir and compared performance with established C-band GMFs. To the best of our knowledge, no studies have used SAR to extract wind direction over lakes. Therefore, it remains uncertain if SAR-based wind retrieval methods can be reliably applied to lakes.

The recently launched Surface Water Ocean Topography (SWOT) Ka-band SAR interferometer was designed to retrieve water surface elevations from lakes $(250\ m)^2$ (science requirement) or larger (Fu et al., 2024), having a nominal resolution of 22 m. Compared to the side-looking geometry and centimeter-scale wavelength of satellites often used for wind estimation (such as the 5.5 cm wavelength Sentinel-1 C-band SAR, discussed here), SWOT's relatively short Ka-band wavelengths (8.3 mm) and near-nadir viewing geometry could be well-suited to observing smaller surface waves often found on lakes. Preliminary investigations show Ka-band near-nadir backscatter relationships with wind speed are similar to scatterometers, indicating the potential to estimate

10.1029/2024EA003971

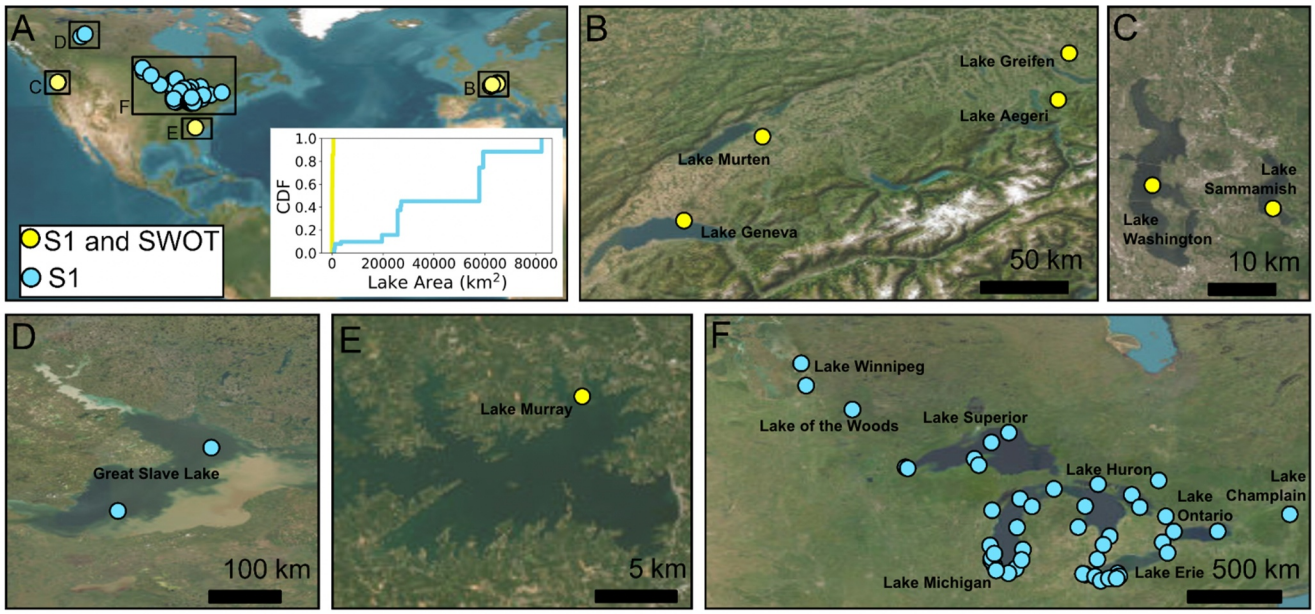

Figure 1. Over water buoy validation dataset included 58 buoys across 19 lakes (a) Validation buoys were mapped according to which satellites had co-located observations. Sentinel-1 had co-located observations at all 58 buoys (19 lakes) and SWOT had co-located observations at seven buoys (seven lakes). The inset CDF plot shows the distribution of lake area (km^2) associated with each buoy grouped according to which satellites had co-located observations. Lake area was repeatedly counted if the lake had more than one buoy (b) Four buoys (4 lakes) were included from Switzerland Swiss DataLakes (c) Two buoys (2 lakes) were included from King County, Washington, US Water and Land Services (d)–(f) 52 buoys (13 lakes) across the USA and Canada were included from NOAA National Data Buoy Center.

wind fields using SWOT (Fayne & Smith, 2023). Wind estimates from SWOT could be useful for characterizing SWOT surface water elevation and extent observation uncertainty.

Uncertainties regarding whether SAR methods developed for wind over ocean environments will transfer to lakes with comparatively short fetches, small waves, and complex topography requires further investigation. This study aims to understand the opportunities and challenges of estimating wind over lakes from SAR and determine if these approaches are generalizable across satellites with different frequencies. Therefore, we use Sentinel-1 C-band and SWOT Ka-band imagery to investigate backscatter phenomenology over lakes with the following objectives: (a) characterize the occurrence of wind streaks observed in SAR imagery over lakes, (b) estimate wind direction and speed using SAR backscatter, and (c) validate estimates at over-water buoys.

2. Materials and Methods

2.1. Study Areas

The study areas were selected by identifying lakes represented in the SWOT Prior Lake Database (Wang et al., 2025, in press) that had buoys equipped with anemometers to observe wind speed and direction during 2023–2024 and that were larger than the minimum area required to estimate wind direction (1 km^2) (see Section 2.4) (Figure 1). Based on this criteria, 19 lakes in North America and Europe were included, ranging in size from 7 to 82,220 km^2 with a median area of 1,121 km^2. Lakes are located in a temperate climate except for the Great Slave Lake, which is located in a boreal climate. All lakes are naturally occurring and experience ice formation except for Lake Murray which is a reservoir used for hydropower.

2.2. Datasets

2.2.1. Surface Water Ocean Topography Dataset

We retrieved Ka-band backscatter (sigma0) data from the SWOT Level 2 Water Mask Raster Image Data Product version C at 100 m resolution (Surface Water Ocean Topography, 2024). SWOT repeat orbit is 21 days but revisit time can be as often as 4 days at the mid latitudes (Biancamaria et al., 2016). The data is composed of a 120 km

23335084, 2025, 3, Downloaded from https://agupubs.onlinelibrary.wiley.com/doi/10.1029/2024EA003971, Wiley Online Library on [04/04/2025]. See the Terms and Conditions (https://onlinelibrary.wiley.com/terms-and-conditions) on Wiley Online Library for rules of use; OA articles are governed by the applicable Creative Commons License

23335084, 2025, 3, Downloaded from https://agupubs.onlinelibrary.wiley.com/doi/10.1029/2024EA003971, Wiley Online Library on [04/04/2025]. See the Terms and Conditions (https://onlinelibrary.wiley.com/terms-and-conditions) on Wiley Online Library for rules of use; OA articles are governed by the applicable Creative Commons License

swath with a 20 km gap at nadir. One side of the swath is HH polarized and the other side is VV polarized (Biancamaria et al., 2016). Backscatter images were delivered with preprocessing steps already applied, including radiometric and atmospheric calibration (JPL internal document, 2024). We removed pixels flagged as 'bad' quality from images. We included backscatter (sigma0) images from January to March of 2024 for analysis. There were no SWOT images with co-temporal buoy observations in 2023.

2.2.2. Sentinel-1 Dataset

We retrieved Sentinel-1 (S1) C-band data from the S1 interferometric wide swath (IW) ground range detected product at 10 m resolution with 12 day repeat orbit on Google Earth Engine (GEE) (Earth Engine Data Catalog, 2024). This product is delivered by GEE with preprocessing steps already applied (e.g., noise removal, radiometric calibration, terrain calibration) to derive backscatter (Google for Developers, 2024). We selected VV polarized images for their compatibility with the CMOD5.N GMF (a full description of the GMF is available in Section 2.5) and resampled the images using nearest neighbors to 100 m resolution to match SWOT image resolution and reduce speckles. Images from January 2023 to March of 2024 were included in our analysis.

2.2.3. In-Situ Buoy Dataset

We obtained in situ wind speed and direction observations from over water buoys to validate SAR-derived wind fields. In total, 58 buoys across 19 lakes in North America and Europe were included from three sources, including NOAA (NOAA National Data Buoy Center, 1971) (52 buoys, 13 lakes), King County, Washington, US Water and Land Services (King County, 2024) (2 buoys, 2 lakes), and Swiss DataLakes (Datalakes, 2024) (4 buoys, 4 lakes) (Figure 1). Buoy wind speeds were observed using anemometers at different heights (1–10 m). Differences between anemometer height from the ground and modeled wind speed height must be taken into account for equivalent comparisons. Since most anemometer heights were below 10 m, we converted wind speed to 10 m height for consistency with wind speeds modeled from SAR (see Section 2.5) using a simple logarithmic wind profile equation defined as

$$U(z) = U(z_m) \times \ln(z/z_0) \,/\, \ln(z_m/z_0) \quad (1)$$

where z_0 is the roughness length (typical value of 1.52×10^{-4} m), z is the target height of 10 m, z_m is the anemometer height, U (z_m) is the measured buoy wind speed, and U(z) is the estimated wind speed at 10 m height (Lu et al., 2018; Sergeev et al., 2023). This conversion resulted in an average difference of 0.31 m/s between original and 10 m buoy wind speeds. Four NOAA buoys did not provide anemometer height, so the mean height of all other buoys was used instead. Temporal sampling varied by buoy from one to 60 minutes. Complete buoy information can be found in Table S1 in Supporting Information S1.

2.2.4. Reanalysis Dataset

We used wind fields from the European Center for Medium-Range Weather Forecasts (ECMWF) Reanalysis v5 (ERA5) dataset to benchmark the improvement of our SAR-based estimates over existing global reanalysis data. ERA5 is the fifth generation ECMWF reanalysis for global climate and weather available hourly at a 0.25° resolution (Hersbach et al., 2018). While local datasets tend to be higher resolution, we chose ERA5 for its global coverage since this analysis spanned three countries (USA, Canada, Switzerland) and presented methods that are globally applicable. We use the 10 m speed and direction products for this analysis.

2.3. Analyze Wind Streak Frequency

Wind streaks in SAR backscatter images can be used to extract wind direction; however, they are not always easy to detect (Zhao et al., 2016). Wind streaks are necessary to extract reliable wind direction from SAR backscatter using the LG method but it is unclear how often they are present in SAR imagery over lakes. We quantified the frequency of wind streaks in S1 and SWOT images and the conditions under which they were observed. While automatic methods using deep learning have been applied to identify wind streaks, they require large training data sets (Wang et al., 2020). More commonly, a visual approach is applied, involving expert inspection of SAR images to manually identify wind streaks (Lehner et al., 1998; Levy, 2001; Zhao et al., 2016). In this study, we used the visual approach to quantify the frequency of visible wind streaks in S1 and SWOT images. It should be

23335084, 2025, 3, Downloaded from https://agupubs.onlinelibrary.wiley.com/doi/10.1029/2024EA003971, Wiley Online Library on [04/04/2025]. See the Terms and Conditions (https://onlinelibrary.wiley.com/terms-and-conditions) on Wiley Online Library for rules of use; OA articles are governed by the applicable Creative Commons License

noted, however, that the visual approach may lead to a conservative identification of wind streaks because visibility can be subject to the range of values used to render the image. Therefore, the thoroughness of the visual wind streak detection does not affect wind direction estimation using the LG-Method (see Section 2.4). For each buoy, we identified co-located images with an overpass occurring within 1 hour of a buoy observation (buoy-image pairs) and recorded the presence/absence of wind streaks at the buoy location. We excluded buoy-image pairs from analysis if ice was present within the water body on the day of the observation. We used the Sentinel-3 derived Daily Lake Ice Extent product with 500 m resolution from the Copernicus Land Monitoring System to identify lake ice extents (European Commission Directorate-General Joint Research Centre, 2024; Heinilä et al., 2021). This filtering process produced 4–13 SWOT images and 2–144 S1 images for analysis at each buoy, and a total of 1,540 buoy-image pairs with wind streak presence/absence records from January 2023–March 2024. Note that wind streak frequency at each buoy is not spatially independent because some lakes have multiple buoys that were observed within the same image. We tested for statistical differences in the distribution of buoy-derived wind speeds and lake fetches, grouped by wind streak presence or absence, using the nonparametric Mann Whitney test (Mann & Whitney, 1947). We defined fetch as the maximum distance that wind in a given direction can travel across the lake surface. We calculated lake fetch for each buoy-image pair using the buoy wind direction measurement and the PLD water body extent.

2.4. Estimate Wind Direction

We retrieved wind direction over lakes from S1 and SWOT using the Modified LG method (LG-Mod) (Rana et al., 2015). The LG method works by evaluating local gradients in backscatter images caused by wind streaks (Koch, 2004). Wind streaks are ideally constant in the direction of the wind and vary the strongest in the direction orthogonal to the wind. Therefore, the gradient describes the direction of the strongest increase, and is orthogonal to the wind direction. While gradients can be found in any direction due to the noise inherent to SAR images, gradients tend to be oriented in the correct orthogonal direction based on the wind streak.

In the LG-Mod method, images are typically resampled between 100 and 400 m to reduce speckle and enhance visualization of wind streaks (Koch, 2004; Rana et al., 2015; Wang & Li, 2016). Then the study area is divided into subimages, or regions of interest (ROIs), corresponding to the user's desired output grid. Local gradients are calculated by applying the optimized derivative Sobel operator to backscatter images in linear scale. Gradients corresponding to unusable points are discarded (i.e., pixels corresponding to land), and then the main wind direction and associated marginal error parameter (ME) can be extracted in each ROI. The marginal error parameter is calculated using a (1-α) confidence interval and used as an indicator of the reliability of the wind direction estimate. Regions of interest with less directional variability have a smaller ME and likely a more accurate direction. Therefore, the ME can be used to exclude unreliable directions by setting an acceptance angular threshold, ME^{TH}. For a full explanation of LG-Mod, see Rana et al. (2015).

We estimated wind direction at 1 km resolution and the associated ME with a 95% confidence interval. This means each ROI was 1 km by 1 km and consisted of 100 m resolution pixels (i.e., 100 pixels in each ROI). Wind direction was only estimated in ROIs where at least 40% of pixels were within the water body boundary. While it is ideal to estimate wind direction in ROIs with wind streaks, we estimated wind direction in ROIs without wind streaks as well because the visual method of identifying wind streaks may be conservative. LG-Mod wind directions have an inherent 180° ambiguity, whereby they can determine the wind orientation but not the wind origin. Hereafter, wind direction estimated from SAR using LG-Mod are referred to as S1 wind direction or SWOT wind direction, respective to the satellite used.

2.5. Estimate Wind Speed

CMOD5.N is a C-band GMF defining the empirical relationship between C-band backscatter sensed by the ERS-2 and ASCAT scatterometers and equivalent neutral 10 m ocean winds (i.e., wind speed at neutral atmospheric conditions) (Hersbach, 2010). Differences between lake and ocean environments with respect to GMFs are fetch, water temperature, and salinity, which have a weak influence on the first-order relationship between backscatter and wind speeds (Donelan & Pierson, 1987). So, despite the development of CMOD5.N for use over the ocean, we expect the first-order relationship between backscatter and wind speed will be similar over lakes. We estimated wind speed at 100 m resolution by inverting CMOD5.N using S1 backscatter data, the S1 wind direction data relative to azimuth, and incidence angle. S1 wind direction estimates used in the wind speed calculation were

23335084, 2025, 3, Downloaded from https://agupubs.onlinelibrary.wiley.com/doi/10.1029/2024EA003971, Wiley Online Library on [04/04/2025]. See the Terms and Conditions (https://onlinelibrary.wiley.com/terms-and-conditions) on Wiley Online Library for rules of use; OA articles are governed by the applicable Creative Commons License

downscaled from 1 to 100 m resolution to match the S1 backscatter data resolution. Hereafter, wind speeds estimated from S1 with CMOD5.N and LG-Mod are referred to as S1 wind speeds.

GMFs for SWOT Ka-band winds are under development to complement the mission's low-rate ocean observations (Fayne, 2023, 2024; Stiles et al., 2024). But they are in early stages, and so were not incorporated into this analysis. Instead, we conducted a preliminary analysis of the relationship between SWOT backscatter, incidence angle, and wind speed. First, we extracted SWOT backscatter and incidence angle at buoy locations with co-temporal wind speed observations within 1 hour of satellite overpass. This point-wise comparison yielded 66 observations with limited representation of SWOT backscatter across the full range of wind speeds and incidence angles. We then conducted a complementary analysis using ERA5 wind speeds for direct comparison. We extracted the median SWOT backscatter, incidence angle and ERA5 wind speed from water bodies included in this study using all SWOT images included in the analysis (Number of observations = 447).

2.6. Validate Wind Field Estimates

We validated wind fields estimated from SAR using buoy observations and benchmarked the improvement over ERA5. For validation, we selected wind fields with co-located buoy observations within 1 hour of satellite overpass and extracted the wind field value at the buoy location (Figure 1). We did not account for atmospheric stability in buoy observations, but the average difference between neutral and non-neutral wind speeds is low (~0.2 m/s), and likely has minimal influence on our estimates (Hersbach, 2010; Rana et al., 2019). We evaluated wind direction performance with 180° ambiguity in order to quantify skill at extracting wind streak orientation and because, given ERA5's coarseness, it was largely ineffective at identifying the correct wind direction. Considering the 18° ambiguity, we evaluated wind direction performance using the mean absolute error (MAE). We evaluated wind speed performance using mean bias error (MBE), MAE, and root mean square error (RMSE). We compared the performance of SAR wind direction and speed to ERA5 performance. A total of 66 SWOT and 1474 S1 buoy-image pairs were used for wind direction validation. A total of 1474 S1 image-buoy pairs were used for wind speed validation.

To understand what lake or buoy conditions were associated with better performance, we calculated the Pearson correlation coefficient between the wind error and a variety of lake, buoy, and radar characteristics including buoy wind speed (m/s), buoy wind direction (degrees), buoy distance to shore (km), lake fetch (km), lake area (km^2), sigma0, incidence angle (degrees), and time difference between buoy observation and satellite overpass (seconds). Only wind estimates filtered using the angular threshold $ME^{TH} = 30°$ were included in this analysis.

We also tested these methods using 10 m resolution S1 images but the performance was worse than that from 100 m resolution S1 images (Table S2 in Supporting Information S1), likely because the resampling reduced speckle noises and improved the overall signal-to-noise ratio (SNR) of the original SAR images. Therefore, we chose to present results from our analysis using 100 m resolution S1 and SWOT images in the main text.

3. Results

3.1. Wind Streak Frequency Analsysis

We quantified the frequency of wind streaks observed by SWOT and S1 (Figure 2). Wind streaks were visible in 13.7% of all buoy-image pairs, and observed more frequently by S1 (14.3%, 211/1474) than SWOT (0%, 0/66). Wind streaks were more frequently observed at higher wind speeds and on lakes with longer fetches. The median wind speed of buoy-image pairs with wind streaks (5.6 m/s) was significantly faster ($p < 0.0001$) than without wind streaks (2.2 m/s). The median lake fetch of buoy-image pairs with wind streaks (125.6 km) was significantly longer ($p < 0.0001$) than without wind streaks (7.9 km). The median wind speed (2.7 m/s) and lake fetch (13.4 km) of S1 image-buoy pairs was faster and longer compared to SWOT median wind speed (1.4 m/s) and lake fetch (2.6 km).

3.2. Wind Direction Analysis

We assessed the performance of SAR-based wind direction with 180° ambiguity according to satellite, angular threshold ME^{TH}, and wind streak presence. SWOT wind direction performance improved with stricter ME^{TH}, ranging from a MAE of 37.9° using all observations to 28.1° using $ME^{TH} = 20°$ (Table 1). In comparison, S1 wind

10.1029/2024EA003971

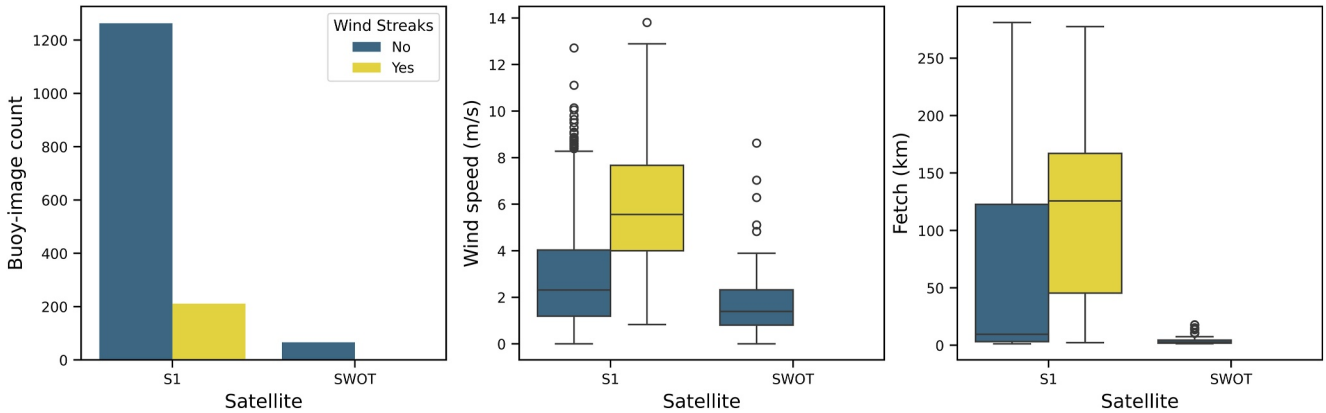

Figure 2. Wind streak summary (a) The number of co-located satellite images with buoy observations within 1 hour of satellite overpass (buoy-image pairs) were grouped according to satellite and wind streak presence (b) The distributions of buoy wind speed (m/s) and (c) lake fetch (km) were grouped according to satellite and wind streak presence.

direction performance did not improve with stricter ME^{TH} but did improve when filtered to observations with wind streaks, reducing MAE from 40.4 to 31.0° (Table 1).

SAR-based wind direction performance was also compared to ERA5 performance, based on the same subsets of buoy wind direction observations for a direct comparison. S1 and SWOT wind direction were more accurate at a higher resolution than ERA5 wind direction. SWOT wind direction performed better than ERA5 in all cases, while S1 wind direction performed better than ERA5 in all cases except when filtering using $ME^{TH} = 20$ with wind streaks (Table 1). We attempted to identify lake and buoy characteristics associated with better wind direction performance; however, none of the characteristics yielded a significant relationship ($p \leq 0.05$) (Figure S1 in Supporting Information S1).

In Figure 3, we mapped S1 wind direction at 1 km resolution over Lake Ontario to highlight the improved representation of within lake wind direction using LG-Mod compared to ERA5. Prominent wind streaks were oriented east-west along the western shore that were aligned with buoy wind direction of 265° (Figure 3a). S1 wind direction aligned closely with wind streaks and the buoy wind direction. The most reliable wind directions with the lowest ME were found along the western shore of the lake where wind streaks were the most prominent. In comparison, the least reliable wind directions with the highest ME were found in the southeastern portion of the

Table 1
Wind Direction Performance Calculated With 180° Ambiguity Grouped According to Satellite, Angular Threshold ME^{TH}, and Presence of Wind Streaks

Image subset	N	LG-mod MAE (degrees)	ERA5 MAE (degrees)
SWOT	66	37.93	39.78
SWOT ($ME^{TH} = 40$)	31	37.54	41.26
SWOT ($ME^{TH} = 30$)	24	34.78	40.32
SWOT ($ME^{TH} = 20$)	10	28.13	50.38
S1	1,474	40.42	41.28
S1 ($ME^{TH} = 40$)	397	38.53	41.38
S1 ($ME^{TH} = 30$)	289	40.09	41.88
S1 ($ME^{TH} = 20$)	94	40.38	41.19
S1 (Wind streaks)	211	34.13	36.46
S1 (Wind streaks, $ME^{TH} = 40$)	61	32	32.75
S1 (Wind streaks, $ME^{TH} = 30$)	44	33.41	35.63
S1 (Wind streaks, $ME^{TH} = 20$)	12	31.04	22.77

23335084, 2025, 3, Downloaded from https://agupubs.onlinelibrary.wiley.com/doi/10.1029/2024EA003971, Wiley Online Library on [04/04/2025]. See the Terms and Conditions (https://onlinelibrary.wiley.com/terms-and-conditions) on Wiley Online Library for rules of use; OA articles are governed by the applicable Creative Commons License

10.1029/2024EA003971

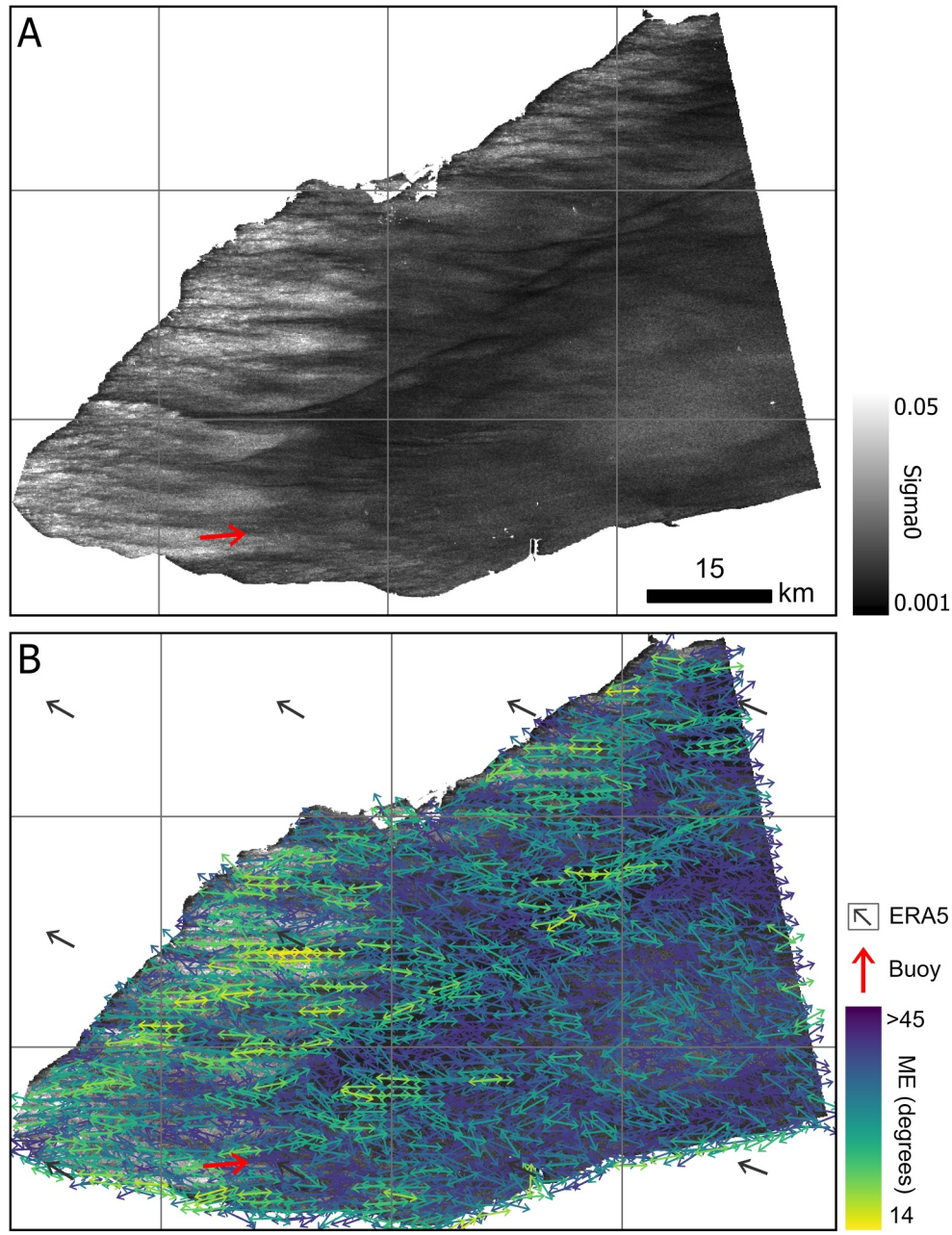

Figure 3. Wind streaks inform S1 wind direction (a) S1 backscatter (linear scale, resampled to 100 m resolution) over a western portion of Lake Ontario on 2023-05-20 with visible wind streaks along the western shore (b) Wind direction and ME (degrees, in 1 km grid) estimated from S1 backscatter using LG-Mod. Arrows represent the wind direction and arrow color represents the ME (degrees). Buoy wind direction shown by the red arrow (265°). ERA5 wind direction pixels (0.25° grid) and arrows shown in gray.

lake where wind streaks were not found, demonstrating the utility of the method to identify regions with and without wind streaks.

SAR-based wind direction also performed well on small lakes. In Figure 4, we map SWOT wind direction over Lake Greifen (7.9 km^2) to demonstrate the improved capability of SAR-based wind direction to resolve small lakes that are a fraction of the size of a single ERA5 grid cell. While wind streaks were difficult to discern visually, LG-Mod was able to retrieve wind direction closely aligned with the buoy wind direction of 123° (see more discussion in Section 4).

23335084, 2025, 3, Downloaded from https://agupubs.onlinelibrary.wiley.com/doi/10.1029/2024EA003971, Wiley Online Library on [04/04/2025]. See the Terms and Conditions (https://onlinelibrary.wiley.com/terms-and-conditions) on Wiley Online Library for rules of use; OA articles are governed by the applicable Creative Commons License

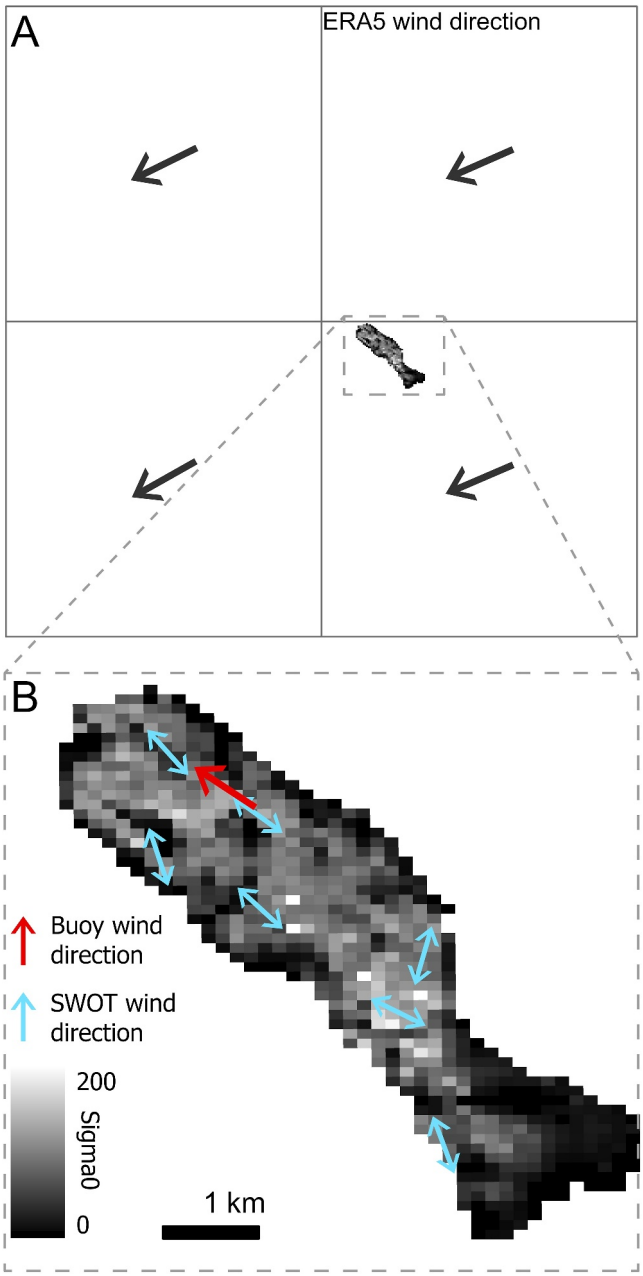

Figure 4. SWOT wind direction compared to ERA5 (a) ERA5 grid cells (0.25°) with wind direction represented by black arrows. Lake Greifen is located in the bottom right grid cell (b) SWOT wind direction (1 km scale) estimated over Lake Greifen on 2024-03-17 is shown using blue arrows. Buoy wind direction shown using the red arrow (123°).

3.3. Wind Speed Analysis

We assessed the performance of S1 wind speed according to ME^{TH} and wind streak presence. Performance improved when filtering with stricter ME^{TH} and improved further when filtering to only include observations with wind streaks (Table 2). Mean absolute error ranged from 2.09 m/s to 1.05 m/s, RMSE ranged from 3.14 m/s to 1.36 m/s, and MBE ranged from 1.38 m/s to −0.27 m/s (Table 2).

S1 wind speed performance was compared with ERA5 based on the same subsets of buoy wind speed observations for a direct comparison. Performance without any filtering, where 85% of estimates did not have wind streaks present, was similar to ERA5. S1 wind speed MAE and RMSE were lower than ERA5 across most subsets (Table 2), with an average decrease in MAE and RMSE of 0.46 m/s and 0.22 m/s, respectively. ERA5 and S1 wind speeds were consistently positively biased (with the only exception from S1 with wind streaks) and bias magnitude decreased with stricter ME^{TH} (Table 2). Based on least squares linear model fits between observed and modeled wind speed, we find S1 captured more wind speed variability with an R^2 of 0.417 ($p < 0.0001$) compared to ERA5 with an R^2 of 0.28 ($p < 0.0001$) (Figure 5). Overall, S1 wind speed showed better agreement with buoy observations than ERA5 (Table 2, Figure 5). Higher wind speed, longer lake fetch, larger lake area, greater buoy distance to shore, smaller sigma0, and larger time difference between buoy and satellite observations were weakly but significantly correlated ($p \leq 0.05$) with smaller wind speed errors (Figure S1 in Supporting Information S1).

Figure 6 illustrates the benefits and challenges of estimating wind from SAR by mapping S1 wind direction (1 km) and wind speed (100 m) on Lake Washington in Seattle. Synthetic aperture radar observations captured spatial variations in wind speeds over the long and narrow arms of Lake Washington, including low wind speeds in the northern portion and higher wind speeds in the middle and southern portions. The most reliable wind direction estimates were found in the middle of the lake corresponding closely with wind streak orientation and buoy wind direction. However, erroneous S1 wind speed and direction estimates were found near the lake shore and at the locations of bridges extending over the lake, highlighting the sensitivity of these methods to non-water pixels.

In the absence of a published SWOT GMF for high-rate data, we assessed the relationship between SWOT backscatter, incidence angle, and wind speed. There were limited comparisons of SWOT observations with cotemporal buoy observations at higher wind speeds and in the smallest incidence angle bin, 0.5–1.5 (Figure 7). However, the relationship between SWOT backscatter, incidence angle, and wind speed were similar between the point-scale buoy wind speed dataset and the waterbody-scale ERA5 wind speed dataset. This correspondence gives us confidence in the ERA5 patterns, despite the limited accuracy of the ERA5 wind speeds reported in Table 2. SWOT backscatter increased with wind speed in the largest incidence angle bin (3.5–4.5°) (Figure 7). In contrast, it decreased with wind speed in the smallest incidence angle bin (0.5–1.5°). There was no discernible trend in the incidence angle bins from 1.5 to 3.5.

4. Discussion

This study finds that SAR can provide useful estimates of wind speed and direction over lakes. While the methods used in this study were originally developed for oceanic and coastal applications, they transfer well to lakes. We find that there are multiple benefits of retrieving wind from SAR. First, wind speed and direction estimates from

23335084, 2025, 3, Downloaded from https://agupubs.onlinelibrary.wiley.com/doi/10.1029/2024EA003971, Wiley Online Library on [04/04/2025]. See the Terms and Conditions (https://onlinelibrary.wiley.com/terms-and-conditions) on Wiley Online Library for rules of use; OA articles are governed by the applicable Creative Commons License

23335084, 2025, 3, Downloaded from https://agupubs.onlinelibrary.wiley.com/doi/10.1029/2024EA003971, Wiley Online Library on [04/04/2025]. See the Terms and Conditions (https://onlinelibrary.wiley.com/terms-and-conditions) on Wiley Online Library for rules of use; OA articles are governed by the applicable Creative Commons License

Table 2
S1 and ERA5 Wind Speed Performance Grouped According to ME^{TH} and Wind Streak Presence

		MBE (m/s)		MAE (m/s)		RMSE (m/s)	
Image subset	N	CMOD5.N + LG-Mod	ERA5	CMOD5.N + LG-Mod	ERA5	CMOD5.N + LG-Mod	ERA5
S1	1,474	1.38	1.39	1.95	2.24	2.82	2.72
S1 (ME^{TH} = 40)	397	1.36	1.27	1.87	2.17	2.81	2.67
S1 (ME^{TH} = 30)	289	1.19	1.2	1.74	2.17	2.62	2.67
S1 (ME^{TH} = 20)	94	0.99	1.43	1.52	2.35	2.09	2.8
S1 (Wind streaks)	211	1.03	0.4	2.09	2.08	3.14	2.68
S1 (Wind streaks, ME^{TH} = 40)	61	0.28	0.9	1.29	2.0	1.99	2.51
S1 (Wind streaks, ME^{TH} = 30)	44	0.23	0.67	1.16	1.85	1.63	2.34
S1 (Wind streaks, ME^{TH} = 20)	12	−0.27	0.73	1.05	1.49	1.36	1.81

SWOT and S1 achieve better accuracy at higher spatial resolution compared to the global reanalysis dataset, ERA5 (Tables 1 and 2). Second, the higher spatial resolution of SAR-based winds allows for observation of considerably more wind variability within lakes than is possible from global reanalysis datasets or a single buoy (Figures 3, 4 and 6). This could be especially beneficial for observing small lakes, lakes with complex shapes, and lakes where local conditions cause wind to shift quickly (Brunet et al., 2023). For example, S1 observations identify low winds in a small part of Lake Washington, which would otherwise be difficult to resolve using reanalysis datasets and buoys because of its complex shape and surrounding topography, located west of the Puget Sound and east of the Cascade mountain range (Figure 6).

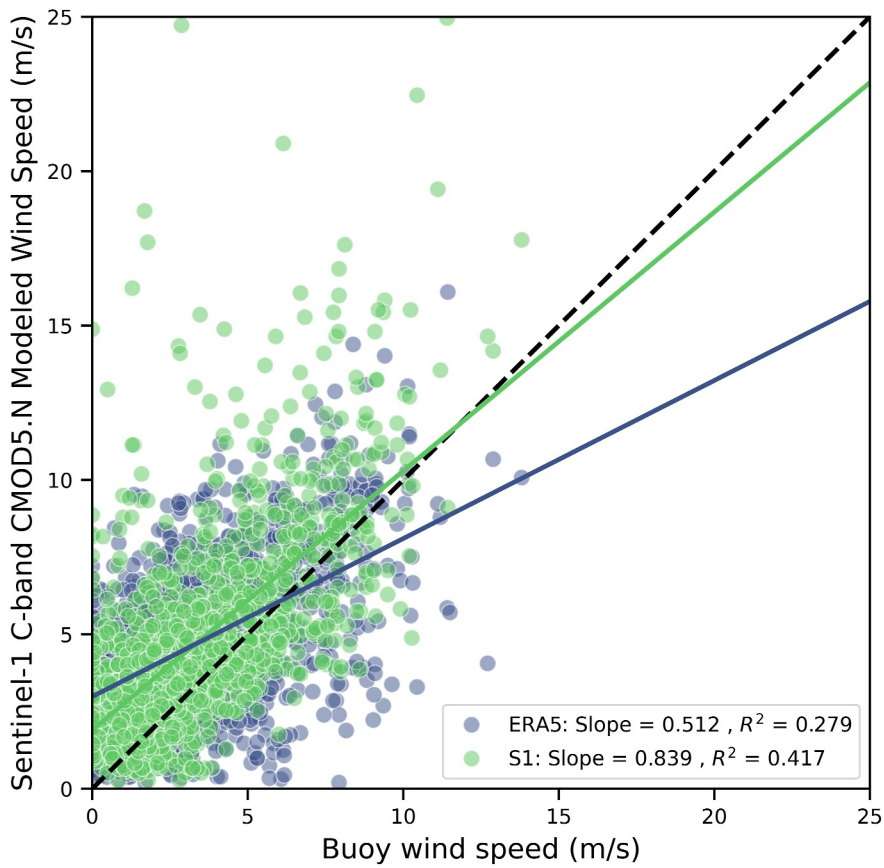

Figure 5. S1 and ERA5 wind speed (m/s) compared to buoy observations. Least squares linear model fits between modeled and observed wind speed plotted for S1 and ERA5. The black dashed line represents a 1:1 relationship.

10.1029/2024EA003971

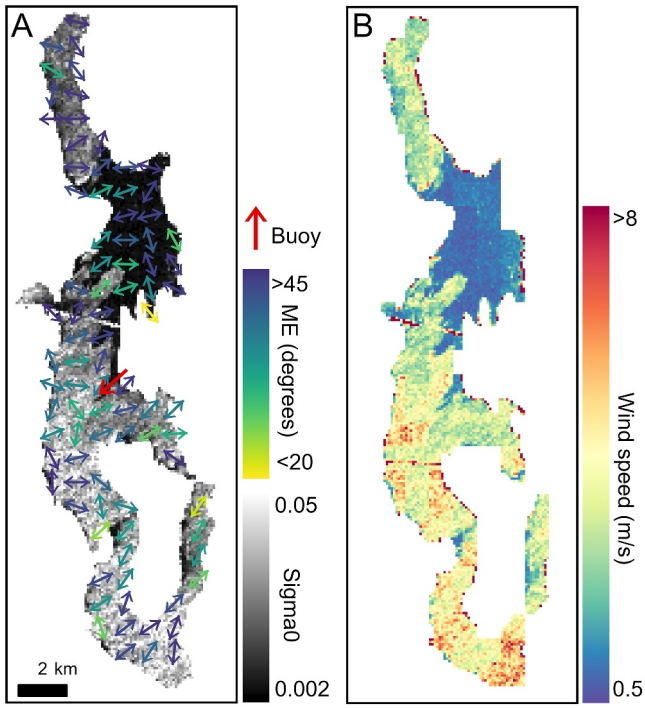

Figure 6. Wind direction and speed from S1 (a) S1 derived wind direction (1 km) and (b) wind speed (100 m) on 2023-03-21 over Lake Washington. Arrows indicate wind direction and are colored according to ME (degrees). Wind speed (m/s) was estimated from S1 backscatter and wind direction using CMOD5.N. The measured buoy wind speed on this date is 5.49 m/s.

To our knowledge, this study is the first large-scale assessment of SAR-based wind over lakes. Lake buoy stations are limited, resulting in 58 available buoys for validation with a minimum lake size of seven km^2 (Figure 1). This limitation, however, underscores the value of leveraging SAR for wind estimation over lakes. The methods applied here could readily be applied globally to inform our understanding of wind and its role driving lake dynamics, especially in data poor regions (Desai et al., 2009; Jalil et al., 2019; Woolway et al., 2019; Zhao et al., 2024).

Despite differences between S1 and SWOT radar instruments, both datasets perform similarly estimating winds. One notable difference is the prevalence that wind streaks are observed by each satellite. S1 observes wind streaks in 14% of buoy-image pairs, which is toward the lower end of the range reported over the ocean, from 12.8% to 70% (Figure 2) (Lehner et al., 1998; Levy, 2001; Wang et al., 2020; Zhao et al., 2016). In contrast, SWOT observes wind streaks in 0% of buoy-image pairs. However, this does not necessarily imply that SWOT is less sensitive to wind-driven roughness, but is likely due to there being a fraction of SWOT observations compared to S1 observations and also the fact that the buoys with available SWOT observations are located on smaller lakes with shorter fetches and slower wind speeds compared to S1 (Figure 2). Since wind streaks are more commonly observed at higher wind speeds and in environments with longer fetches, the lack of observations by SWOT is unsurprising, as is the frequency of S1 observations compared to observations over the ocean (Wang et al., 2020). One other notable difference between the satellites is that the SWOT wind direction performance improved with stricter ME^{TH} while S1 stayed approximately the same (Table 1). Low ME is ideally a result of wind streaks but can be the result of any phenomena on the lake surface that creates a strong gradient or less gradient variability. S1 likely did not improve because ME associated with S1 wind direction was influenced by non-wind features more easily observed on large lakes (i.e., gravity waves, eddies, currents, and circulation patterns driven by thermal difference, density difference, and

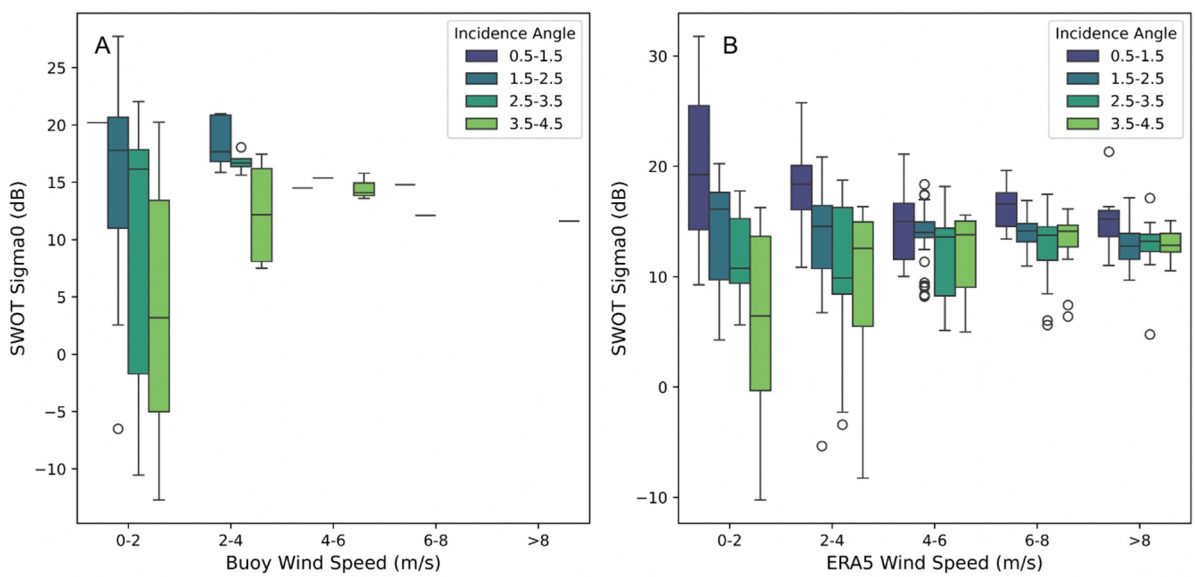

Figure 7. Relationship between Surface Water Ocean Topography (SWOT) backscatter, incidence angle, and wind speed (a) Point comparisons of SWOT backscatter (dB) binned according to buoy wind speed (m/s) and incidence angle (degrees) (b) Median water body comparisons of SWOT backscatter (dB) binned according to ERA5 wind speed and incidence angle (degrees).

23335084, 2025, 3, Downloaded from https://agupubs.onlinelibrary.wiley.com/doi/10.1029/2024EA003971, Wiley Online Library on [04/04/2025]. See the Terms and Conditions (https://onlinelibrary.wiley.com/terms-and-conditions) on Wiley Online Library for rules of use; OA articles are governed by the applicable Creative Commons License

23335084, 2025, 3, Downloaded from https://agupubs.onlinelibrary.wiley.com/doi/10.1029/2024EA003971, Wiley Online Library on [04/04/2025]. See the Terms and Conditions (https://onlinelibrary.wiley.com/terms-and-conditions) on Wiley Online Library for rules of use; OA articles are governed by the applicable Creative Commons License

the interactions with lake shores and barriers). Overall, both datasets appear well suited to observe wind over lakes.

S1 and SWOT wind directions are more accurate than ERA5 and comparable to the accuracy reported from SAR studies in coastal regions (Rana et al., 2015, 2019). Wind direction estimated using LG-Mod from Envisat at 3.6 km resolution and validated with two buoys in coastal Wales had an RMSE ranging from 20 to 44° (Rana et al., 2015). Also using LG-Mod, wind direction estimated from S1 at 12.5 km resolution and validated using buoys in the Camargue and Wadden Sea, regions with complex geomorphology and shallow water depths, had an RMSE ranging from 9 to 15° (Rana et al., 2019). Other studies have applied variants of the LG method and report RMSE ranging from approximately 17 to 36°, which aligns with our MAE ranging from approximately 28 to 40° (Table 1) (Koch, 2004; Wang & Li, 2016; Zhou et al., 2017). Unlike those studies, we report accuracy with an 180° ambiguity due to the difficulty of using ERA5 data to resolve ambiguity in the SAR-based wind direction estimates. Over the ocean, ambiguity is typically resolved using NWP directions, which has worked well because those datasets are accurate over the ocean, and even used as training and validation datasets for GMFs (Wang & Li, 2016). We attempt to resolve ambiguity of SAR based wind direction over lakes using ERA5, but find that it was no more accurate than wind direction estimated from SAR itself, and therefore, not effective for removing 180° ambiguity (Table 1). A primary reason to estimate wind direction from SAR is as an input to a wind speed GMF. Wind speed GMFs are most sensitive to the upwind/downwind or crosswind orientation relative to satellite azimuth, so wind direction with 180° ambiguity is still useful (Hersbach, 2010). Even so, future work should seek to remove this ambiguity more effectively. For example, it is possible that lake seiches, which could be observed using SWOT elevation data, or wind shadows could be used to remove ambiguity.

Wind direction performance is sensitive to directional content but not to the tested lake or buoy characteristics. Directional content refers to the strength of the signal in the backscatter images which can be used to indicate wind direction (Rana et al., 2015). We identify directional content in two ways, including the presence/absence of wind streaks and ME estimates, which are based on the alignment of local directions within an ROI. Consistent with other studies, we find that greater directional content improves wind direction performance for both satellites (Rana et al., 2015, 2019). Interestingly, LG-Mod returns accurate estimates even when gradients are difficult to visually discern (Figure 4). Therefore, we may be underestimating the wind streak frequency based on what we can see compared to what the algorithm can identify (Rana et al., 2015). This is evidenced by the improvement of SWOT wind direction performance with stricter ME thresholds (an indication of increasing directional content), despite no visually identified observations of wind streaks (Figure 2, Table 1). We did not find any significant relationships between wind direction error and lake or buoy characteristics (Figure S1 in Supporting Information S1). While other variables could be influential, we believe a large reason for errors is noise in backscatter resulting in erroneous gradients.

SAR wind speed estimates over lakes are more accurate than ERA5 but not as accurate as estimates over the ocean (Carvajal et al., 2014; Rana et al., 2019; Sergeev et al., 2023; Verspeek et al., 2010). This is unsurprising since CMOD5.N was developed for oceanic use (Hersbach, 2010). Although limited research has been conducted estimating wind speed from SAR over lakes, our results are consistent with those studies (Table 2). Sergeev et al. (2023) used S1 with CMOD5.N to retrieve wind speed over the Gorsky reservoir (430 km^2) with an RMSE ranging from 0.96 to 1.5 m/s and a bias ranging from −0.22 to −1.1 m/s. Katona and Bartsch (2018) used S1 to develop a new empirical model to retrieve wind speed over five small lakes in central Europe with RMSE ranging from 0.9 to 2.6 m/s. Difference in lake size could contribute to the better performance at the larger Gorsky reservoir compared to five small lakes. Similarly, we find better wind speed accuracy on larger lakes, with longer fetches, and faster wind speeds, conditions that more closely resemble those over the ocean (Supplementary Figure S1 in Supporting Information S1). S1 wind speed accuracy increases when filtered to only include observations with wind streaks (Table 2). This improvement is likely due to more accurate wind direction (Table 1) and the tendency of wind streaks to be observed at higher wind speeds.

Although CMOD5.N has better wind speed performance compared to ERA5, we do not necessarily advocate for the application of GMFs developed for the ocean to lakes. Ideally, GMFs should be tailored for lake environments to account for the complexity of lake size and fetch. Particularly with the launch of satellite missions like SWOT that are aimed at observing inland water bodies, methods and models to extract paired observations of wind with surface water extent and height could open new avenues to understand lake dynamics and observation uncertainty at the global scale.

23335084, 2025, 3, Downloaded from https://agupubs.onlinelibrary.wiley.com/doi/10.1029/2024EA003971, Wiley Online Library on [04/04/2025]. See the Terms and Conditions (https://onlinelibrary.wiley.com/terms-and-conditions) on Wiley Online Library for rules of use; OA articles are governed by the applicable Creative Commons License

Our analysis shows that SWOT backscatter is sensitive to wind speed, highlighting its applicability for developing a GMF for lakes (Figure 7). The lower range of incidence angles shows a pattern of increasing SWOT backscatter with increasing wind speed, which aligns with patterns observed from co-temporal AirSWOT (the airborne complement to SWOT) backscatter and ERA5 wind speed (Fayne & Smith, 2023). In contrast, SWOT backscatter decreased with wind speed in the higher range of incidence angles. This is consistent with relationships observed between aircraft Ka-band scatterometer data and near surface wind speed in coastal areas and the open ocean (Vandemark et al., 2004). The recently developed SWOT GMF for coastal and oceanic applications predicts wind speed using SWOT backscatter, incidence angle, and significant wave height (Stiles et al., 2024) and validation using collocated measurements from the ASCAT ocean wind scatterometer onboard MetOP-B and C reports bias ranging from −0.31 m/s to −0.25 m/s (Stiles et al., 2024). SWOT high-rate products that observe inland water bodies, including the raster and pixel cloud, do not include estimates of significant wave height, which makes it difficult to apply this model in the same way we did CMOD5.N. Further, it may be unnecessary to include significant wave height in a GMF tailored to inland water bodies because they experience smaller wave heights. Additional observations of SWOT backscatter across a range of incident angles, azimuths, lake sizes and shapes, wind speeds and directions are needed to further understand these complex relationships, identify important factors, and eventually fit a GMF.

Despite the limited temporal resolution of wind from SAR relative to buoys or reanalysis datasets, there are a number of applications for which it is useful and provides novel insights. First, the increased spatial resolution is necessary to represent wind variability within lakes, which would be otherwise impossible from coarse reanalysis datasets (Figure 6). Additionally, SAR-based wind fields could be used to improve model representation of wind over lakes through data assimilation. For SWOT specifically, estimates of wind speed could be used to characterize uncertainty of SWOT water surface elevation and extent (Fayne & Smith, 2023).

Several challenges remain in applying SAR to estimate wind over lakes. First, a directional signal is necessary to retrieve reliable wind direction. We find wind streaks in only 14% of observations, and even if underestimated, leaves times when other datasets would be necessary to fill in the gaps (Figure 2). Additionally, backscatter images capture many lake phenomena other than wind streaks, including circulation patterns, river inlets or outlets, anthropogenic usage, and infrastructure from our built environment (Figure 6) (Hamze-Ziabari et al., 2022). Methods to retrieve wind are sensitive to these phenomena and can lead to erroneous estimates. Implementing the ME threshold is one example of a strategy that has been proposed to deal with this challenge but it is not perfect (Rana et al., 2015). For example, wind direction estimates over Lake Washington are sensitive to the strong linear signal of bridges crossing the lake, leading to multiple conflicting wind direction estimates (Figure 6). Existing wind speed GMFs (based on C-band SAR) are sensitive to high backscatter returns (Hersbach, 2010), which often correlate with non-water or double bounce pixels. In the same Lake Washington example, extremely high wind speeds are estimated from S1 along the lake shore and bridge due to high backscatter of non-water features and future applications should be careful to mask non-water pixels.

5. Conclusions

This study assessed the utility of SAR, specifically from Sentinel-1 and SWOT satellites, to estimate wind over lakes. Our findings suggest SAR can be used to estimate wind speed and direction at the water-air interface with better accuracy and higher spatial resolution compared to a global reanalysis dataset, ERA5. SWOT and S1 wind direction MAE ranged from 28 to 40° with better performance on subsets with greater directional content. S1 wind speed MAE ranged from 1.05 to 2.09 m/s with better performance on subsets with greater directional content, longer fetches, and faster wind speeds. The relatively high resolution enables direct observation of smaller lakes as well as more detailed observations of within lake variability over large and complexly shaped lakes. While information on wind over lakes is currently limited, SAR has the potential to retrieve high quality information on wind over lakes at a global scale, and may be particularly useful in data scarce regions. SWOT is particularly well suited for this task, and the relationships identified between SWOT backscatter, incidence angle, and wind speed over lakes demonstrate SWOT sensitivity to wind speed. These observations can be useful to inform our understanding of dynamic lake processes and conditions, like evaporation, greenhouse gas emissions, and water quality. Future work to develop wind speed models specifically for lake environments is crucial for reliable retrievals of wind speed across lakes of all shapes and sizes.

23335084, 2025, 3, Downloaded from https://agupubs.onlinelibrary.wiley.com/doi/10.1029/2024EA003971, Wiley Online Library on [04/04/2025]. See the Terms and Conditions (https://onlinelibrary.wiley.com/terms-and-conditions) on Wiley Online Library for rules of use; OA articles are governed by the applicable Creative Commons License

Data Availability Statement

All data used in this study is publicly available online. Sentinel-1 data was downloaded from GEE (Earth Engine Data Catalog, 2024). Surface Water Ocean Topography data was downloaded from PO.DAAC (Surface Water Ocean Topography, 2024). ERA5 data was downloaded from Copernicus (Hersbach et al., 2018). Buoy data from NOAA was downloaded from the National Data Buoy Center (NOAA National Data Buoy Center, 1971). Buoy data from King County, Washington, Water and Land Services was downloaded from (King County, 2024). Buoy data from Swiss DataLakes was downloaded from (Datalakes, 2024). Sentinel-3 derived Daily Lake Ice Extent product was downloaded from the Copernicus Land Monitoring System (European Commission Directorate-General Joint Research Centre, 2024; Heinilä et al., 2021). Code used for this analysis was uploaded to Zenodo (McQuillan, 2024).

Acknowledgments
This research was partially supported by a Virginia Tech Presidential Postdoctoral Fellowship, NASA Water Resources Program (Grant 80NSSC22K0933), and NASA SWOT Science Team (Grant 80NSSC24K1663).

References

Asiyabi, R. M., Ghorbanian, A., Tameh, S. N., Amani, M., Jin, S., & Mohammadzadeh, A. (2023). Synthetic aperture radar (SAR) for ocean: A review. *Ieee Journal of Selected Topics in Applied Earth Observations and Remote Sensing*, *16*, 9106–9138. https://doi.org/10.1109/JSTARS.2023.3310363

Baracchini, T., Hummel, S., Verlaan, M., Cimatoribus, A., Wüest, A., & Bouffard, D. (2020). An automated calibration framework and open source tools for 3D lake hydrodynamic models. *Environmental Modelling and Software*, *134*, 104787. https://doi.org/10.1016/j.envsoft.2020.104787

Biancamaria, S., Lettenmaier, D. P., & Pavelsky, T. M. (2016). The SWOT mission and its capabilities for land hydrology. In A. Cazenave, N. Champollion, J. Benveniste, & J. Chen (Eds.), *Remote sensing and water Resources* (pp. 117–147). Springer International Publishing. https://doi.org/10.1007/978-3-319-32449-4_6

Brunet, D., Valipour, R., & Rao, Y. R. (2023). Wind variability over a large lake with complex topography: Lake of the Woods. *Journal of Great Lakes Research*, *49*(1), 112–121. https://doi.org/10.1016/j.jglr.2022.08.019

Bruun Christiansen, M., Koch, W., Horstmann, J., Bay Hasager, C., & Nielsen, M. (2006). Wind resource assessment from C-band SAR. *Remote Sensing of Environment*, *105*(1), 68–81. https://doi.org/10.1016/j.rse.2006.06.005

Carvajal, G. K., Eriksson, L. E. B., & Ulander, L. M. H. (2014). Retrieval and quality assessment of wind velocity vectors on the ocean with C-band SAR. *IEEE Transactions on Geoscience and Remote Sensing*, *52*(5), 2519–2537. https://doi.org/10.1109/TGRS.2013.2262377

Chelton, D. B., & Freilich, M. H. (2005). Scatterometer-based assessment of 10-m wind analyses from the operational ECMWF and NCEP numerical weather prediction models. *Monthly Weather Review*, *133*(2), 409–429. https://doi.org/10.1175/MWR-2861.1

Chen, C., Xu, Q., Ralph, E., Budd, J. W., & Lin, H. (2004). Response of Lake superior to mesoscale wind forcing: A comparison between currents driven by QuikSCAT and buoy winds. *Journal of Geophysical Research*, *109*(C10). https://doi.org/10.1029/2002JC001692

Datalakes. (2024). Search, visualise and download data on Swiss lakes. [Dataset] Retrieved from https://www.datalakes-eawag.ch/

Desai, A. R., Austin, J. A., Bennington, V., & McKinley, G. A. (2009). Stronger winds over a large lake in response to weakening air-to-lake temperature gradient. *Nature Geoscience*, *2*(12), 855–858. https://doi.org/10.1038/ngeo693

Donelan, M. A., & Pierson, W. J., Jr. (1987). Radar scattering and equilibrium ranges in wind-generated waves with application to scatterometry. *Journal of Geophysical Research*, *92*(C5), 4971–5029. https://doi.org/10.1029/JC092iC05p04971

Earth Engine Data Catalog. (2024). Sentinel-1 SAR GRD: C-Band synthetic aperture radar ground range detected, log scaling. *Google for Developers*. [Dataset] Retrieved from https://developers.google.com/earth-engine/datasets/catalog/COPERNICUS_S1_G

European Commission Directorate-General Joint Research Centre. (2024). Lake ice extent 2021-present (raster 500 m), northern hemisphere, daily—Version 1. [Dataset] Retrieved from https://land.copernicus.vgt.vito.be/geonetwork/srv/api/records/clms_global_lie_500m_v1_daily

Fayne, J. V. (2023). Inland water inundation extent and wind speeds from passive L-band GNSS-R and active C- and ka-band radar. In *2023 international conference on electromagnetics in advanced applications (ICEAA)*. https://doi.org/10.1109/ICEAA57318.2023.10297651.574

Fayne, J. V. (2024). SWOT phenomenology for lakes and wetlands. In *Abstract presented at IEEE IGARSS 2024*.

Fayne, J. V., & Smith, L. C. (2023). How does wind influence near-nadir and low-incidence ka-band radar backscatter and coherence from small inland water bodies? *Remote Sensing*, *15*(13), 3361. Article 13. https://doi.org/10.3390/rs15133361

Fu, L.-L., Pavelsky, T., Cretaux, J.-F., Morrow, R., Farrar, J. T., Vaze, P., et al. (2024). The surface water and ocean Topography mission: A breakthrough in radar remote sensing of the ocean and land surface water. *Geophysical Research Letters*, *51*(4), e2023GL107652. https://doi.org/10.1029/2023GL107652

Gelaro, R., McCarty, W., Suárez, M. J., Todling, R., Molod, A., Takacs, L., et al. (2017). The modern-era retrospective analysis for research and applications, version 2 (MERRA-2). *Journal of Climate*, *30*(14), 5419–5454. https://doi.org/10.1175/JCLI-D-16-0758.1

Gerling, T. W. (1986). Structure of the surface wind field from the Seasat SAR. *Journal of Geophysical Research*, *91*(C2), 2308–2320. https://doi.org/10.1029/JC091iC02p02308

Google for Developers. (2024). Sentinel-1 algorithms. Retrieved from https://developers.google.com/earth-engine/guides/sentinel1

Hamze-Ziabari, S. M., Foroughan, M., Lemmin, U., & Barry, D. A. (2022). Monitoring mesoscale to submesoscale processes in large lakes with sentinel-1 SAR imagery: The case of Lake geneva. *Remote Sensing*, *14*(19), 4967. Article 19. https://doi.org/10.3390/rs14194967

Heinilä, K., Mattila, O.-P., Metsämäki, S., Väkevä, S., Luojus, K., Schwaizer, G., & Koponen, S. (2021). A novel method for detecting lake ice cover using optical satellite data. *International Journal of Applied Earth Observation and Geoinformation*, *104*, 102566. https://doi.org/10.1016/j.jag.2021.102566

Hersbach, H. (2010). Comparison of C-band scatterometer CMOD5.N equivalent neutral winds with ECMWF. *Journal of Atmospheric and Oceanic Technology*, *27*(4), 721–736. https://doi.org/10.1175/2009JTECHO698.1

Hersbach, H., Bell, B., Berrisford, P., Biavati, G., Horanyi, A., Munoz Sabater, J., et al. (2018). ERA5 hourly data on single levels from 1940 to present. *Copernicus Climate Change Service (C3S) Climate Data Store (CDS)*. [Dataset]. https://doi.org/10.24381/CDS.ADBB2D47

Hofmann, H., Federwisch, L., & Peeters, F. (2010). Wave-induced release of methane: Littoral zones as source of methane in lakes. *Limnology & Oceanography*, *55*(5), 1990–2000. https://doi.org/10.4319/lo.2010.55.5.1990

Jalil, A., Li, Y., Zhang, K., Gao, X., Wang, W., Khan, H. O. S., et al. (2019). Wind-induced hydrodynamic changes impact on sediment resuspension for large, shallow Lake Taihu, China. *International Journal of Sediment Research*, *34*(3), 205–215. https://doi.org/10.1016/j.ijsrc.2018.11.003

Jang, J.-C., Park, K.-A., Mouche, A. A., Chapron, B., & Lee, J.-H. (2019). Validation of Sea surface wind from sentinel-1A/B SAR data in the coastal regions of the Korean peninsula. *Ieee Journal of Selected Topics in Applied Earth Observations and Remote Sensing*, *12*(7), 2513–2529. https://doi.org/10.1109/JSTARS.2019.2911127

Jin, K.-R., & Wang, K.-H. (1998). Wind generated waves in lake Okeechobee1. *JAWRA Journal of the American Water Resources Association*, *34*(5), 1099–1108. https://doi.org/10.1111/j.1752-1688.1998.tb04157.x

JPL internal document. (2024). Surface water and ocean Topography mission (SWOT) project: SWOT Level 2 KaRIn high rate raster product description, revision B. JPL D-56416, october 26, 2023. Retrieved from https://archive.podaac.earthdata.nasa.gov/podaac-ops-cumulus-docs/web-misc/swot_mission_docs/pdd/D-56416_SWOT_Product_Description_L2_HR_Raster_20231026_RevBcite.pdf

Katona, T., & Bartsch, A. (2018). Estimation of wind speed over lakes in Central Europe using spaceborne C-band SAR. *European Journal of Remote Sensing*, *51*(1), 921–931. https://doi.org/10.1080/22797254.2018.1516516

Keen, C. S., & Lyons, W. A. (1978). Lake/Land breeze circulations on the western shore of Lake Michigan. *Journal of Applied Meteorology and Climatology*, *17*(12), 1843–1855. https://doi.org/10.1175/1520-0450(1978)017<1843:LBCOTW>2.0.CO;2

King County. (2024). Lake buoy data. [Dataset] Retrieved from https://green2.kingcounty.gov/lake-buoy/default.aspx

Koch, W. (2004). Directional analysis of SAR images aiming at wind direction. *IEEE Transactions on Geoscience and Remote Sensing*, *42*(4), 702–710. https://doi.org/10.1109/TGRS.2003.818811

Lehner, S., Horstmann, J., Koch, W., & Rosenthal, W. (1998). Mesoscale wind measurements using recalibrated ERS SAR images. *Journal of Geophysical Research*, *103*(C4), 7847–7856. https://doi.org/10.1029/97JC02726

Lemmin, U., & D'Adamo, N. (1997). Summertime winds and direct cyclonic circulation: Observations from Lake Geneva. *Annales Geophysicae*, *14*(11), 1207–1220. https://doi.org/10.1007/s00585-996-1207-z

Levy, G. (2001). Boundary layer roll statistics from SAR. *Geophysical Research Letters*, *28*(10), 1993–1995. https://doi.org/10.1029/2000GL012667

Lu, Y., Zhang, B., Perrie, W., Mouche, A. A., Li, X., & Wang, H. (2018). A C-band geophysical model function for determining coastal wind speed using synthetic aperture radar. *Ieee Journal of Selected Topics in Applied Earth Observations and Remote Sensing*, *11*(7), 2417–2428. https://doi.org/10.1109/JSTARS.2018.2836661

Mann, H. B., & Whitney, D. R. (1947). On a test of whether one of two random variables is stochastically larger than the other. *The Annals of Mathematical Statistics*, *18*(1), 50–60. https://doi.org/10.1214/aoms/1177730491

Mao, M., van der Westhuysen, A. J., Xia, M., Schwab, D. J., & Chawla, A. (2016). Modeling wind waves from deep to shallow waters in Lake Michigan using unstructured SWAN. *Journal of Geophysical Research: Oceans*, *121*(6), 3836–3865. https://doi.org/10.1002/2015JC011340

McQuillan, K. A. (2024). kmcquil/Wind_Over_Lakes_With_SAR: V1.0.0: December 20, 2024 release (Version 1.0.0) [Software]. *Zenodo*. https://doi.org/10.5281/zenodo.14536380

Messager, M. L., Lehner, B., Grill, G., Nedeva, I., & Schmitt, O. (2016). Estimating the volume and age of water stored in global lakes using a geo-statistical approach. *Nature Communications*, *7*(1), 13603. https://doi.org/10.1038/ncomms13603

Monaldo, F. M., Thompson, D. R., Pichel, W. G., & Clemente-Colon, P. (2004). A systematic comparison of QuikSCAT and SAR ocean surface wind speeds. *IEEE Transactions on Geoscience and Remote Sensing*, *42*(2), 283–291. https://doi.org/10.1109/TGRS.2003.817213

Nghiem, S. V., Leshkevich, G. A., & Stiles, B. W. (2004). Wind fields over the Great lakes measured by the SeaWinds scatterometer on the QuikSCAT satellite. *Journal of Great Lakes Research*, *30*(1), 148–165. https://doi.org/10.1016/S0380-1330(04)70337-8

NOAA National Data Buoy Center. (1971). Meteorological and oceanographic data collected from the national data buoy center coastal-marine automated network (C-man) and moored (weather) buoys. NOAA National Centers for Environmental Information. [Dataset] Retrieved from https://www.ncei.noaa.gov/archive/accession/NDBC-CMANWx. Accessed 01 01 2024.

Rana, F. M., Adamo, M., Lucas, R., & Blonda, P. (2019). Sea surface wind retrieval in coastal areas by means of Sentinel-1 and numerical weather prediction model data. *Remote Sensing of Environment*, *225*, 379–391. https://doi.org/10.1016/j.rse.2019.03.019

Rana, F. M., Adamo, M., Pasquariello, G., De Carolis, G., & Morelli, S. (2015). LG-mod: A modified local gradient (LG) method to retrieve SAR Sea surface wind directions in marine coastal areas. *Journal of Sensors*, *2016*, 9565208. https://doi.org/10.1155/2016/9565208

Schilder, J., Bastviken, D., van Hardenbroek, M., Kankaala, P., Rinta, P., Stötter, T., & Heiri, O. (2013). Spatial heterogeneity and lake morphology affect diffusive greenhouse gas emission estimates of lakes. *Geophysical Research Letters*, *40*(21), 5752–5756. https://doi.org/10.1002/2013GL057669

Sergeev, D., Ermakova, O., Rusakov, N., Poplavsky, E., & Gladskikh, D. (2023). Verification of C-band geophysical model function for wind speed retrieval in the open ocean and inland water conditions. *Geosciences*, *13*(12), 361. Article 12. https://doi.org/10.3390/geosciences13120361

Stiles, B. W., Fore, A. G., Bohe, A., Chen, A. C., Chen, C. W., Molero, B., & Dubois, P. (2024). Ocean surface wind speed retrieval for SWOT KA-band radar interferometer. In *Abstracted presented at IEEE IGARSS 2024*.

Surface Water Ocean Topography. (2024). SWOT Level 2 water mask raster image data product. *Version C. Ver. C [Dataset] PO.DAAC, CA, USA*. https://doi.org/10.5067/SWOT-RASTER-2.0

Tammeorg, O., Niemistö, J., Möls, T., Laugaste, R., Panksep, K., & Kangur, K. (2013). Wind-induced sediment resuspension as a potential factor sustaining eutrophication in large and shallow Lake Peipsi. *Aquatic Sciences*, *75*(4), 559–570. https://doi.org/10.1007/s00027-013-0300-0

Trolle, D., Staehr, P. A., Davidson, T. A., Bjerring, R., Lauridsen, T. L., Søndergaard, M., & Jeppesen, E. (2012). Seasonal dynamics of CO2 flux across the surface of shallow temperate lakes. *Ecosystems*, *15*(2), 336–347. https://doi.org/10.1007/s10021-011-9513-z

Vandemark, D., Chapron, B., Sun, J., Crescenti, G. H., & Graber, H. C. (2004). Ocean wave slope observations using radar backscatter and laser altimeters. *Journal of Physical Oceanography*, *34*(12), 2825–2842. https://doi.org/10.1175/JPO2663.1

Verspeek, J., Stoffelen, A., Portabella, M., Bonekamp, H., Anderson, C., & Saldana, J. F. (2010). Validation and calibration of ASCAT using CMOD5.n. *IEEE Transactions on Geoscience and Remote Sensing*, *48*(1), 386–395. https://doi.org/10.1109/TGRS.2009.2027896

Wang, B., Chen, D., & Song, M. (2022). Study on the applicability of ERA5 reanalysis data at lake taihu. *Journal of Geoscience and Environment Protection*, *10*(12), 1–16. Article 12. https://doi.org/10.4236/gep.2022.1012001

Wang, C., Vandemark, D., Mouche, A., Chapron, B., Li, H., & Foster, R. C. (2020a). An assessment of marine atmospheric boundary layer roll detection using Sentinel-1 SAR data. *Remote Sensing of Environment*, *250*, 112031. https://doi.org/10.1016/j.rse.2020.112031

Wang, H., Kaisam, J. P., Liang, D., Deng, Y., & Shen, Y. (2020b). Wind impacts on suspended sediment transport in the largest freshwater lake of China. *Hydrology Research*, *51*(4), 815–832. https://doi.org/10.2166/nh.2020.153

23335084, 2025, 3, Downloaded from https://agupubs.onlinelibrary.wiley.com/doi/10.1029/2024EA003971, Wiley Online Library on [04/04/2025]. See the Terms and Conditions (https://onlinelibrary.wiley.com/terms-and-conditions) on Wiley Online Library for rules of use; OA articles are governed by the applicable Creative Commons License

Wang, J., Pottier, C., Cazals, C., Battude, M., Sheng, Y., Song, C., et al. (2025). The Surface Water and Ocean Topography mission (SWOT) Prior Lake Database (PLD): Lake mask and operational auxiliaries. *Water Resources Research*, *61*, e2023WR036896. https://doi.org/10.1029/2023WR036896. (in press).

Wang, Y.-R., & Li, X.-M. (2016). Derivation of Sea surface wind directions from TerraSAR-X data using the local gradient method. *Remote Sensing*, *8*(1), 53. Article 1. https://doi.org/10.3390/rs8010053

Woolway, R. I., Merchant, C. J., Van Den Hoek, J., Azorin-Molina, C., Nõges, P., Laas, A., et al. (2019). Northern hemisphere atmospheric stilling accelerates lake thermal responses to a warming world. *Geophysical Research Letters*, *46*(21), 11983–11992. https://doi.org/10.1029/2019GL082752

Zecchetto, S. (2018). Wind direction extraction from SAR in coastal areas. *Remote Sensing*, *10*(2), 261. Article 2. https://doi.org/10.3390/rs10020261

Zhao, B., Huntington, J., Pearson, C., Zhao, G., Ott, T., Zhu, J., et al. (2024). Developing a general Daily Lake evaporation model and demonstrating its application in the state of Texas. *Water Resources Research*, *60*(3), e2023WR036181. https://doi.org/10.1029/2023WR036181

Zhao, Y., Li, X.-M., & Sha, J. (2016). Sea surface wind streaks in spaceborne synthetic aperture radar imagery. *Journal of Geophysical Research: Oceans*, *121*(9), 6731–6741. https://doi.org/10.1002/2016JC012040

Zhou, L., Zheng, G., Li, X., Yang, J., Ren, L., Chen, P., et al. (2017). An improved local gradient method for Sea surface wind direction retrieval from SAR imagery. *Remote Sensing*, *9*(7), 671. Article 7. https://doi.org/10.3390/rs9070671

23335084, 2025, 3, Downloaded from https://agupubs.onlinelibrary.wiley.com/doi/10.1029/2024EA003971, Wiley Online Library on [04/04/2025]. See the Terms and Conditions (https://onlinelibrary.wiley.com/terms-and-conditions) on Wiley Online Library for rules of use; OA articles are governed by the applicable Creative Commons License